CONF-790927--17

LA-UR-79-2499

TITLE: RF QUADRUPOLE BEAM DYNAMICS DESIGN STUDIES

MASTER

AUTHOR(S): K. R. Crandall, R. H. Stokes, and T. P. Wangler

SUBMITTED TO: 1979 Linear Accelerator Conference
Montauk, NY, Sept. 9-14

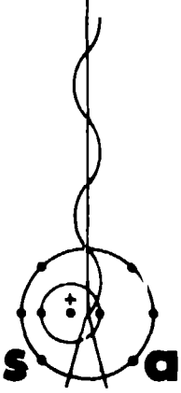

los alamos
scientific laboratory
of the University of California
LOS ALAMOS, NEW MEXICO 87545

Form No. 836
St. No. 2629
1/75

UNITED STATES
ENERGY RESEARCH AND
DEVELOPMENT ADMINISTRATION
CONTRACT W-7405-ENG. 36

1979 LINAC ACCELERATOR CONFERENCE

RF QUADRUPOLE BEAM DYNAMICS DESIGN STUDIES*

K. R. Crandall, R. H. Stokes, and T. P. Wangler
Los Alamos Scientific Laboratory
Los Alamos, New Mexico 87545

Summary

The radio-frequency quadrupole (RFQ) linear accelerator structure is expected to permit considerable flexibility in achieving linac design objectives at low velocities. Calculational studies show that the RFQ can accept a high-current, low-velocity, dc beam, bunch it with high efficiency, and accelerate it to a velocity suitable for injection into a drift-tube linac. Although it is relatively easy to generate a satisfactory design for an RFQ linac for low beam currents, the space-charge effects produced by high currents dominate the design criteria. Methods have been developed to generate solutions that make suitable compromises between the effects of emittance growth, transmission efficiency, and overall structure length. Results are given for a test RFQ linac operating at 425 MHz.

Introduction

Soon after the linear accelerator was invented, searches began for methods to circumvent the incompatibility between longitudinal and radial stability. The use of drift-tube foils or grids, externally applied fields, and alternating phase focusing has met with success in specific areas of application. However, each of these solutions has serious disadvantages particularly in the acceleration of low-velocity ions. Since 1956, there have been suggestions[1-4] that linear accelerator electric fields could be used for radial focusing as well as for acceleration. These proposals were based on noncylindrically symmetric electrode shapes that would generate transverse quadrupole fields. This rf self-focusing is an important new idea especially at low velocities because the electric force is velocity independent.

In 1970, Kapchinskii and Teplyakov[5,6] (K-T) proposed a particularly attractive form of these new ideas. The previous proposals to generate quadrupole fields used specially shaped gaps between drift tubes or waveguides to generate localized focusing forces. However, the scheme proposed by K-T was a more basic and flexible idea in which the quadrupole focusing field was spatially continuous along the z-axis. We call this structure the RFQ. Figure 1 shows a schematic view of a four-vane resonator that is the form of the RFQ being developed at the Los Alamos Scientific Laboratory (LASL).

The RFQ may have important applications in the low-velocity part of many types of ion accelerators. It can provide several necessary functions in a continuous manner to produce a final beam suitable for injection into a conventional accelerator. Briefly these functions are the following: (1) acceptance of a dc beam (50-keV protons, for example) and radially matching it into the following sections of the RFQ; (2) bunching this beam adiabatically with high capture efficiency (>90%); and (3) accelerating the beam to an energy (1-MeV protons, for example) that is convenient for injection into the next acceleration stage. In this paper we will consider the next stage to be a drift-tube linac. Through proper design it is possible to control the particle distribution in the phase-stable bucket so that nonadiabatic acceleration effects are minimized. Also, the final synchronous phase can be brought to a value (say -30°) that is suitable for capture by a drift-tube linac. Because the radial focusing forces are electric and retain their full strength at low velocity, and also because the forces are spatially continuous, the above functions can be accomplished at low velocities with minimal effects from space charge. Also, as suggested by K-T, space-charge effects can be further minimized through proper control of the bunching process. This idea is an important contribution that is compatible with possible choices of RFQ design parameters.

There are several possible applications of the RFQ now under consideration at LASL. These include: (1) a high-intensity deuteron accelerator for the Hanford Fusion Materials Irradia-

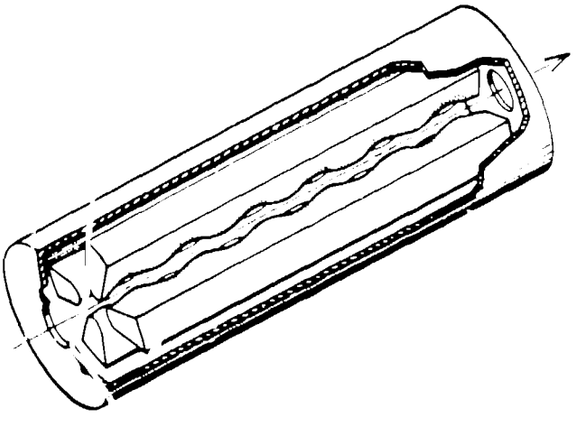

Fig. 1. Four-vane resonator.

*Work performed under the auspices of the U. S. Department of Energy.

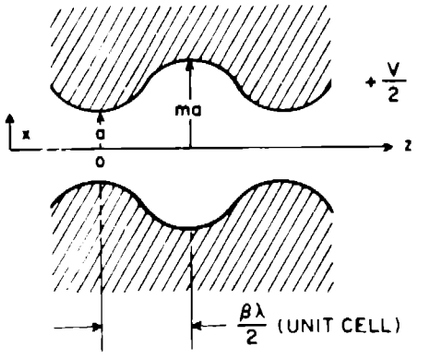

Fig. 2. RFQ pole-tip geometry.

tion Test (FMIT) Facility, (2) the Pion Generator for Medical Irradiation (PIGMI), a high-intensity proton accelerator for use in pion and neutron radiotherapy, (3) a heavy-ion accelerator for inertial fusion, and (4) a high-energy accelerator for ions such as neon. Methods we have found useful in choosing beam-dynamics parameters for RFQ systems are presented. As a specific example, we give the results of these methods applied to a proton linac designed to test the RFQ principle.

RFQ Electric Fields and Pole-Tip Geometry

In the RFQ the electric field distribution is generated by four poles arranged symmetrically around a central z-axis. The poles are excited with rf power so that at a given time, adjacent pole tips have equal voltages of opposite signs. If the pole tips have constant radius as z is varied, then only a transverse field (mainly quadrupole) is present. In the x-z plane for example, this quadrupole field is focusing for one-half of the rf period and defocusing the other half. The structure has the properties of an alternating-gradient focusing system with a strength independent of particle velocity. To generate a longitudinal accelerating field the pole tips are periodically varied in radius. The variation is such that, at a value of z where the pole tips in the x-z plane have minimum radius, the pole tips in the y-z plane have maximum radius. This is shown in Fig. 1. Figure 2 shows a cut through the x-z plane, and shows the mirror symmetry of the opposite poles. In Fig. 2 the radius parameter a, the radius modulation parameter m, and the cell length are defined. The longitudinal field is generated between the x pole tip that has minimum radius at z = 0, and the y pole tip that has minimum radius at z = $\beta\lambda/2$. The unit cell is $\beta\lambda/2$ in length and corresponds to one acceleration gap. Adjacent unit cells have oppositely direct E_z fields, so that in practice only every other cell contains a particle bunch.

In the coordinate system of Fig. 2 the lowest-order potential function given by K-T is written in cylindrical coordinates (r, ψ, z) as follows:

$$U = \frac{V}{2}\left[X\left(\frac{r}{a}\right)^2 \cos 2\psi + AI_o(kr)\cos kz\right] \cdot \sin(\omega t + \phi) \quad , \tag{1}$$

where V is the potential difference between adjacent pole tips, and $k = 2\pi/\beta\lambda$.

From this we obtain the following electric field components:

$$E_r = -\frac{XV}{a^2} r \cos 2\psi - \frac{kAV}{2} I_1(kr)\cos kz \quad , \tag{2}$$

$$E_\psi = \frac{XV}{a^2} r \sin 2\psi \quad , \tag{3}$$

$$E_z = \frac{kAV}{2} I_o(kr)\sin kz \quad , \tag{4}$$

each multiplied by $\sin(\omega t + \phi)$. Our method of calculating RFQ beam dynamics is based on these fields and is described in Ref. 7. The quantities A and X are given by:

$$A = \frac{m^2 - 1}{m^2 I_o(ka) + I_o(mka)} \tag{5}$$

$$X = 1 - AI_o(ka) \quad . \tag{6}$$

The quantity VA is the potential difference that exists on the axis between the beginning and the end of the unit cell. This means that the space-average longitudinal field is given by $E_o = 2AV/\beta\lambda$. The energy gain of a particle with charge q and synchronous velocity βc traversing a unit cell is approximately:

$$\Delta W = qE_o \ell T \cos\phi_s \quad , \tag{7}$$

where $\ell = \beta\lambda/2$, and $T = \pi/4$ is the value of the transit-time factor for a longitudinal field with space variation $\sin kz$. Our notation is similar to K-T except that our A equals their divided by $T = \pi/4$.

A radial stability diagram for the RFQ is given in Fig. 3. The abscissa is given by:

$$\Delta = \frac{\pi^2 qVA \sin\phi}{2Mc^2\beta^2} \quad . \tag{8}$$

This is proportional to the usual "rf defocus" force that gives radial defocusing when a linac

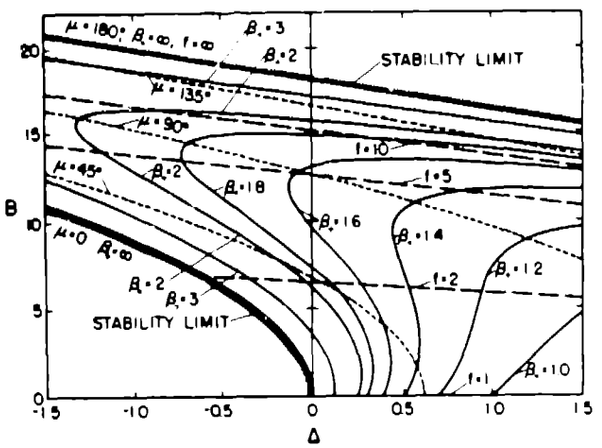

Fig. 3. RFQ radial stability diagram.

is operated with a negative phase angle in the range -90 to 0 degrees. The ordinate in Fig. 3 is:

$$B = \frac{q\lambda^2}{Mc^2} \cdot \frac{XV}{a^2} \quad . \tag{9}$$

This is proportional to the radial focusing force, and depends on the magnitude of the electric quadrupole strength XV/a^2. The electric quadrupole strength does not explicitly depend on z. This means that for given values of a, m, and β, the focusing strength is constant through a unit cell. It also means that one can maintain the same focusing strength in every unit cell by varying the parameters such that XV/a^2 is held fixed. Except for the short, initial, radial matching section, the linac discussed in the section "Design of the 425-MHz RFQ Test" has been designed to have a constant radial-focusing strength. Later we show that this has a geometrical consequence that may be beneficial in the [illegible] of RFQ resonators.

The pole-tip shape required to produce the above electric fields is given by:

$$x^2 - y^2 = r^2 \cos 2\psi = \frac{a^2}{X} \left[1 - AI_o(kr) \cos kz\right] . \tag{10}$$

To obtain the shape of one pole tip in the x-z plane we let $\psi = 0$. This gives:

$$\frac{x^2}{a^2} = \frac{1 - AI_o(kx) \cos kz}{1 - AI_o(ka)} \quad . \tag{11}$$

We then solve this equation numerically to find values of x as a function of z. Call these values of x, which are solutions, $\alpha(z)$. To describe the geometry in the transverse plane we have derived an equation for the transverse radius of curvature of the pole tip. This curvature is:

$$R(z) = \alpha(z) \frac{P + Q}{P - Q} \quad , \tag{12}$$

where

$$P = I_o(ka) + I_o(mka)$$

and

$$Q = \frac{ka^2}{2\alpha} (m^2 - 1) I_1(k\alpha) \cos kz$$

In our pole-tip geometrical design we have made the radius of the pole tips equal to $\alpha(z)$. The pole-tip shape in the transverse plane was approximated by requiring the pole tips to have the radius of curvature R(z). The pole tips are constructed by repeated cuts in the transverse plane by a tape-controlled milling machine. This procedure is discussed more fully in Ref. 8.

At $z = \beta\lambda/4$, half way through the unit cell, the RFQ has quadrupolar symmetry. At this point both the x and y pole tips have a radius equal to $r_o = aX^{-1/2}$. Also, at this point the radius of curvature $R = r_o$. The quantity r_o can be regarded as a characteristic average radius of the RFQ pole tips. As we have discussed, if V is constant, keeping the focusing strength at a fixed value requires X/a^2 to be constant, and also this is equivalent to keeping r_o fixed. In general, a fixed value of r_o can be expected to minimize variations in the vane-to-vane capacitance, and should facilitate the design of an RFQ resonator in which the pole-tip voltage distribution is required to be flat over its entire length.

RFQ Design Procedures

If the ion species and the initial and final energies are given, and if the frequency and intervane potential are specified, the RFQ design is determined when the three independent functions a(z), m(z), and $\phi_s(z)$ are given, where z is the axial distance along the accelerator. Although it may be more convenient to explicitly use other related functions such A, X, or B, the designer must determine three independent functions that produce the desired objectives in terms of adequate radial focusing, capture efficiency, radial emittance growth overall length, or other stated criteria. Simple linear forms for the above functions can achieve these objectives for low beam currents as long as the rate of change of the variables is slow enough to approximate an adiabatic condition. However, as the magnitude of the space-charge force increases, more complex forms for these functions appear to become necessary to minimize both particle loss and radial emittance growth.

One possible solution to this problem has been proposed by K-T. In this method Ω_o, the longitudinal, small oscillation, angular frequency at zero current, and Z_b, the spatial length of the separatrix, are held constant. If the functional form of B is specified, then the three independent functions a, m and ϕ_s are determined. Expressions for Ω_o and Z_b are:

$$\Omega_o^2 = \frac{qVA\lambda^2|\sin\ \phi_s|}{4Mc^2\ 2\pi} \tag{13}$$

$$Z_b = \frac{\beta\lambda\phi}{2\pi} \ , \tag{14}$$

where ϕ is the angular length of the separatrix, which is related to the synchronous phase ϕ_s by:

$$\tan\ \phi_s = \frac{\sin\ \phi - \phi}{1 - \cos} \tag{15}$$

In the region of small longitudinal oscillations and for adiabatic changes, constant Ω_o implies a beam envelope of constant length. For a longitudinally matched beam this also implies an invariant longitudinal charge density distribution and fixed beam length. This result holds for zero current and is also true in the presence of space-charge forces, if one assumes the beam bunch to be uniformly distributed in a three-dimensional ellipsoid of constant dimensions. Constant Z_b together with constant Ω_o can furthermore be shown to make the charge-density distribution approximately constant for large, longitudinal oscillations at zero current. As can be seen from Eqs. (14) and (15), the invariance of Z_b determines ϕ_s (β). Then equation (13) determines A(β).

This method of attempting to keep the charge density distribution approximately constant, while accelerating and bunching in phase, will be expected to reduce those space-charge effects, such as radial emittance growth, that appear to be correlated with longitudinal compression of the beam bunch. However, after the resulting velocity profile $\beta(z)$ is determined, the function A(z) takes on small values, especially for large synchronous phases, and increases very slowly except near the end. This can result in an excessively long structure, particularly as the input synchronous phase approaches $\phi_s = -90^o$. To reduce the length, the initial value of ϕ_s must depart appreciably from -90^o, but this reduces the initial value of ϕ, and results in reduced capture efficiency.

We have explored a generalization of the above method, where we replace the two constants Ω_o and Z_b by the new invariants ε and α, given as:

$$\varepsilon = \frac{-2\pi\dot{\Omega}_o}{\Omega_o^2} \tag{16}$$

and

$$\alpha = \Omega_o Z_b^2 \ . \tag{17}$$

When $\varepsilon = 0$ this reduces to the K-T method. For positive ε the small oscillation frequency Ω_o decreases at a constant percentage rate, and the separatrix length Z_b gradually increases. We expect this approach to yield a charge distribution that can slowly compress or expand in size depending upon the value of ε. In addition, for fixed final values of A and ϕ_s, the overall length decreases as ε increases. Generally we have found acceptable solutions with ε in the range $0 \leq \varepsilon \leq 0.2$.

We find that the use of either the K-T approach or the generalized approach is effective in reducing radial emittance growth, while the beam is being bunched. We refer to this section of the RFQ as the Gentle Bunching Section. We also find that to obtain high capture efficiency, it is necessary to introduce a section before the Gentle Buncher in which the input variables are specified as a function of z rather than β, so that the input synchronous phase can start at $\phi_s = -90^o$ and the initial value of A can be A = 0. In order to reduce the overall length following the Gentle Buncher, we add a section that maintains a high value of A at the final synchronous phase. The remaining problem of radially matching the beam into the time-varying acceptance of the RFQ requires an initial section for matching. We are thus led to four stages in the overall design as shown schematically in Fig. 4. We will now describe the first stage, the Radial Matching Section.

The matched ellipse parameters in the RFQ depend on the rf phase and are relatively independent of position along the linac. Therefore the orientation of the acceptance ellipse depends on time. For proper matching into the RFQ, one must provide a transition from a beam having time-independent characteristics to one that has the proper variations with time. This means that at the input, a time-independent set of ellipse parameters is required. These parameters will depend on the beam current. Our solution is to taper the vanes at the input of the RFQ so that the focusing strength changes from almost zero to its full value over a distance of several (5-10) focusing periods. This procedure allows the time-independent beam to adapt itself to the time structure of the focusing system. Quadrupole symmetry is maintained throughout this section (no vane modulation).

This procedure is illustrated in Fig. 5, a display generated by the program TRACE,[9] which has been modified to include rf quadrupoles,

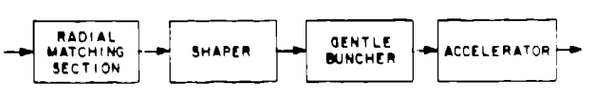

Fig. 4. Functional block diagram.

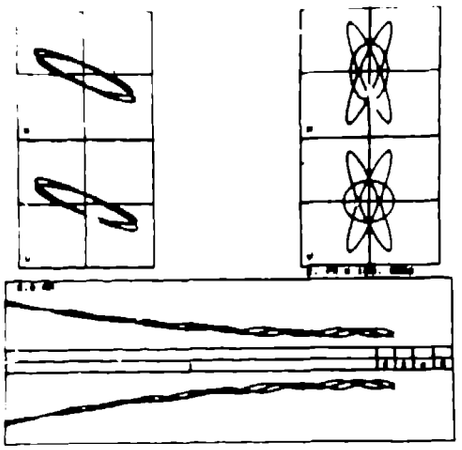

Fig. 5. Radial Matching Section.

either of constant or tapered strengths. The matched ellipse parameters are first found for various phases in the constant-strength section. Three such matched ellipses, corresponding to phases 90° apart, are shown in the upper right side of the figure for both the x-x' and y-y' planes. This graphically demonstrates how different the matched ellipses can be as a function of phase, and also shows the relatively small area of overlap that is common to all of these ellipses. The phase-space plots at the upper left are the result of following these same three ellipses backward through a tapered section of the RFQ, 5-periods long (10 cells). One can see that these ellipses are very similar and have a high degree of overlap. The bottom graph in the figure shows the horizontal and vertical profiles that result from following these three ellipses through the tapered rf quadrupole. Space-charge effects were included in this calculation, which assumed a beam current of 30 mA.

An unexpected benefit of the Radial Matching Section is that the increase in aperture at the input results in weak fringe fields and negligible fringe effects for both longitudinal and radial motions. The longitudinal field generated within the matching section is also negligible because of the fact that the change in B occurs over many rf cycles.

The second stage, which we call the Shaper Section, can begin at $\phi_s = -90°$. The accelerating field is increased steadily from zero, while ϕ_s is maintained at a large value, so as to obtain a high capture efficiency. Under the influence of the rising axial field, an input dc beam with small energy spread will rotate through many cycles of longitudinal oscillation. The filament in phase space wraps around itself to approximate a matched beam in longitudinal phase space. Some compression of the beam within the phase stable area is desirable to anticipate subsequent non adiabatic behavior, which could lead to particle loss. At high beam currents, such compression should be limited, however, because of the large radial emittance growth that can result when the beam is tightly bunched. Even so, dramatic effects of space-charge repulsion will be especially apparent at the first phase foci for an input dc beam with small energy spread.

For the third stage, the Gentle Buncher, we employ the generalized method, where we satisfy equations (16) and (17) and hold B constant. The Gentle Buncher Section completes the bunching begun in the Shaper Section and accelerates the quasi-matched beam from the Shaper, until the final synchronous phase is reached. The bunch length and the charge density undergo no large change in the process.

When the final synchronous phase is reached, the Acceleration Section begins. In this section ϕ_s, m, and a are held at constant final values to apply a relatively large fraction of the intervane voltage on axis, and to bring the beam to its final energy within a short distance.

An important step in the design procedure is a choice of operating intervane potential, which normally should be as large as possible, consistent with the sparking limit. The results from program SUPERFISH[10] show that for the RFQ vanes constructed at LASL, the highest surface fields, E_s, occur in the middle of each cell at the point of pure quadrupole symmetry. The maximum field does not occur at the pole tip, but occurs at the point where the vanes have minimum separation. The field at the pole tip is V/r_o and the peak field $E_s = \kappa V/r_o$ where for our geometry $\kappa = 1.36$. Once the choice of maximum allowable surface field is made, the ratio V/r_o is determined.

After a choice of B is made, which provides a good compromise between radial stability and adequate aperture size, the quantities V and r_o can be obtained from the relations:

$$r_o = \frac{q\lambda^2 E_s}{Mc^2 B\pi^2} \tag{18}$$

$$V = \frac{q\lambda^2 E_s^2}{Mc^2 B \kappa^2} \tag{19}$$

We see that higher surface field E_s and smaller B will increase both r_o and V. The average axial field then becomes:

$$E_o = \frac{2q\lambda A E_s^2}{Mc^2 B \beta \kappa^2} \quad . \tag{20}$$

We choose an initial m value of m = 1. A final value of m 2 produces a good compromise between acceleration efficiency, A, and focusing efficiency, X, at the end. If X is too small the constraint that B is constant may make the final radius parameter too small.

Error Tolerances

After a linac has been designed, one must try to determine how sensitive the design is to all probable sources of error. The quantity and quality of the output beam can be degraded by a variety of things, such as a mismatch and a misteering of the input beam, and alignment errors and excitation errors in the linac. Tolerances can be specified for some of these errors only by running a large number of numerical simulations. For other types of errors, it is possible to make more general statements, and it is these types that we will be concerned with in this section.

The results can be specified in terms of the magnitudes of the multipoles of the focusing field relative to the quadrupole strength at the bore radius. The radial component of the n^{th} multipole at radius, r, and angle, , is defined to be:

$$E_{r,n} = A_n \left(\frac{r}{r_o}\right)^{n-1} \cos\ (n\psi - \delta_n) \quad , \tag{21}$$

where A_n is the amplitude and δ_n is the phase of the n^{th} multipole, and r_o is the bore radius.

The values given below, as well as those given for image charge effects, (see Appendix) were obtained using a computer program that calculates the charge density induced on equipotential surfaces.[11] The unperturbed calculations were made with the vanes approximated by four circular cylinders symmetrically placed about the z-axis. The cylinder walls were a distance r_o from the z-axis and the diameter of each cylinder was $2r_o$.

Alignment Errors

The vanes are displaced slightly from their proper positions. Symmetric displacements of opposite poles, inward or outward, will have no significant effect other than changing the quadrupole strength slightly, which is equivalent to changing the operating voltage. Nonsymmetric displacements will introduce odd-order multipoles. An example of a nonsymmetric displacement is a horizontal displacement of the vertical vanes. A small displacement, d, has been calculated to produce multipoles of order 1, 3, and 5 having fractions of the quadrupole term of 0.16 d/r_o, 0.64 d/r_o, and 0.024 d/r_o, respectively. The dominant term appears to be the sextupole (n = 3), and by placing an acceptable limit on it one can specify a tolerance on d/r_o. If it is desirable to keep the sextupole term below 1%, then the tolerance on d/r_o is approximately 1.5%.

Excitation Errors

The ideal excitation is for the potential on each of the four vanes to oscillate between $\pm V/2$ at all points along the linac. Variations in the potential in the longitudinal direction will probably be gradual and small. Information about the longitudinal field can be obtained from beadpull measurements.

Errors in the transverse fields can be represented most generally by assuming that each vane is oscillating at a different potential. The potential on the i^{th} vane would oscillate between $\pm(V + \Delta V_i)/2$, and the excitation level could be adjusted so that the average potential is correct, which would make

$$\sum_{i=1}^{4} \Delta V_i = 0 \quad . \tag{22}$$

The voltage errors, ΔV_i, can be divided into symmetric and antisymmetric parts. The symmetric components correspond to errors on opposite poles having the same magnitude and the same sign; the antisymmetric components correspond to errors on opposite poles having the same magnitude and opposite signs. The symmetric components have no effect on the multipole spectrum, but the antisymmetric components will generate odd-order multipoles. Let v_x and v_y be the fractional antisymmetric components in the horizontal and vertical vanes, respectively. That is, the potential on the opposing horizontal vanes would oscillate with the magnitudes $(1\pm v_x)V/2$. The magnitudes of the odd multipoles are found to be proportional to $v = (v_x^2 + v_y^2)^{1/2}$, and the ratio of the first four to the quadrupole strengths are given below:

$$A_1/A_2 = 0.397\ v \quad ; \tag{23}$$

$$A_3/A_2 = 0.308\ v \quad ; \tag{24}$$

$$A_5/A_2 = 0.029\ v \quad ; \tag{25}$$

$$A_7/A_2 = 0.041\ v \quad . \tag{26}$$

That is, a 10% antisymmetric component (v = 0.1) would cause a 4% dipole field and a 3% sextupole field. If it is necessary to keep the sextupole

field below 1%, then one must keep $v < 0.037$. The dipole field would simply cause a displacement of the electrical axis of the quadrupole by the same percentage.

Design of the 425-MHz RFQ Test

One of the applications of the RFQ under consideration at LASL is for the high-intensity 35-MeV deuteron accelerator being designed for the Hanford Fusion Materials Irradiation Test (FMIT) Facility to be installed at the Hanford Engineering Development Laboratory (HEDL) at Richland Washington. An important step in evaluation of the RFQ for this linac is a full power test, which uses an existing proton injector and an existing source of rf power. As an example of the design method discussed above, we present the RFQ design for this test, which we will call the 425-MHz Test Design. Table I shows a list of parameters. Because of limitations imposed by the existing hardware, the frequency was chosen at f = 425 MHz and the length was constrained to be equal to L = 110.8 cm.

The surface gradient, E_s, was chosen to have the conservative value 27 MV/m. After the Radial Matching Section, a constant value B = 5.85 provides a compromise between radial stability and tolerance requirements arising from the small aperture. The resulting characteristic average radius is r_o = 0.2 cm and the resulting intervane voltage is V = 44 kV. The objective of the test is to capture a dc beam of energy W_i = 0.1 MeV, bunch and accelerate it to some energy greater than about 0.5 MeV, and to study the performance as a function of input current. The exact value of the final synchronous phase is not important, as long as good bunching can be demonstrated. Two computer programs have been written to help generate parameters for the beam-dynamics program PARMTEQ (see Appendix). The first program generates the Gentle Buncher parameters as a function of axial distance z, given initial and final energies for this section and given the ε parameter. The second program takes the initial Gentle Buncher parameters as final values for the Shaper Section, generates Shaper parameters as a function of z, then traces particles through the Shaper in longitudinal phase space, thus giving an estimate of expected capture efficiency. In addition, both programs calculate several quantities as a function of z, such as the ratio of space charge to focusing force (see Appendix), and longitudinal and radial oscillation frequencies. These results are useful as a guide to predict and interpret subsequent PARMTEQ results.

The chosen design is one with a Gentle Buncher parameter ε = 0, which corresponds to the K-T approach. Several designs made with ε = 0.2 gave comparable results. Figure 6 shows the resulting profiles from PARMTEQ for several variables. The four basic sections of the structure are indicated. The final energy after 110.8 cm and 165 cells is W_f = 0.640 MeV. The radial matching is done in the first ten cells or 5.2 cm, where B is linearly varied from an initial value of B = 0.20 to a final value B = 5.85, and is kept constant throughout the rest of the structure. The slow increase of m during the first half of the structure appears to be necessary in order to reduce radial space-charge effects as was discussed previously. As m increases and the acceleration efficiency A (not shown) also increases, the focusing efficiency, X, decreases. The constant value of B then implies a decrease in the radius parameter a. The transverse acceptance is determined by the final aperture and has a normalized value A_n = 0.09π cm-mr at the nominal current of I = 15 mA. This can be compared with an expected input beam from the ion source having a normalized emittance of E_n = 0.05π cm-mr. The input particle distribution used in the PARMTEQ calculation gave 100% of the beam within this phase-space area, and 90% within a normalized area of 0.034π cm-mr.

In Table II we list the PARMTEQ results for the beam transmission efficiency, the output beam current, and the radial emittance growth. The emittance growth is the normalized emittance of the transmitted beam divided by the normalized emittance of the input beam. Both emittances are obtained from ellipses which

TABLE I

425-MHz TEST DESIGN PARAMETERS

Ion	H^+
Frequency	425 MHz
Input Energy	0.100 MeV
Output Energy	0.640 MeV
Intervane Voltage	44 kV
Minimum Radius Parameter	0.126 cm
Overall Vane Length	110.8 cm
Number of Cells	165
Nominal Current	15 mA

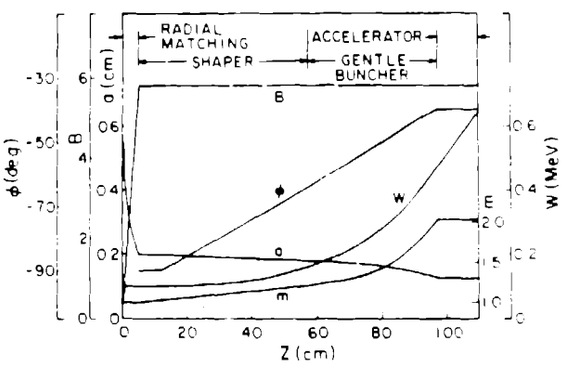

Fig. 6. Parameters for the 425-MHz test design.

TABLE II

RESULTS FROM 425-MHA TEST DESIGN

Input Current (mA)	Transmission Efficiency (%)	Output Current (mA)	Radial Emittance Growth (90% Contour)
0	96.7	0	1.04
15	96.1	14.4	1.13
30	86.4	25.9	1.23
45	73.6	33.1	1.19
60	68.6	41.2	1.22
100	54.4	54.4	1.07

contain 90% of their respective beams. As the input current increases, a larger number of particles is lost radially to the bore, which decreases in size from the input to the output. This selective radial loss explains the decreasing emittance growth for the higher currents.

Figure 7 shows the phase, energy, and radial profiles and the transverse phase space in both planes for I=0 and for the nominal beam current of I=15 mA. The dotted lines on the x profile plot indicate the aperture size. Figure 8 shows the longitudinal phase space at several cells along the RFQ for both I=0 and I=15 mA, starting with an initial dc beam with zero energy spread. Space-charge effects, which become apparent near the first phase focus, persist throughout the remaining I=15 mA plots.

It is of interest to compare the results of our 425-MHz Test Design with those that are obtained by a more simple approach, where, after the initial matching section, ϕ_s is linearly increased from -90° to -40° and the modulation parameter m is linearly ramped from m = 1 to 2 over the total distance of 110.8 cm. We refer to this design as the Linear Ramp Design, and it is characterized by the lack of a Gentle Buncher Section. The Linear Ramp Design gives a larger final energy of W_f = 0.719 MeV in 150 cells, which exceeds that of the 425-MHz Test Design because of a larger average axial field. Results showing the beam transmission efficiency, output current and radial emittance growth for the Linear Ramp Design are presented in Table III.

TABLE III

RESULTS FROM LINEAR RAMP DESIGN

Input Current (mA)	Transmission Efficiency (%)	Output Current (mA)	Radial Emittance Growth (90% Contour)
0	96.9	0	1.12
15	79.2	11.9	1.48
45	41.4	18.6	1.16

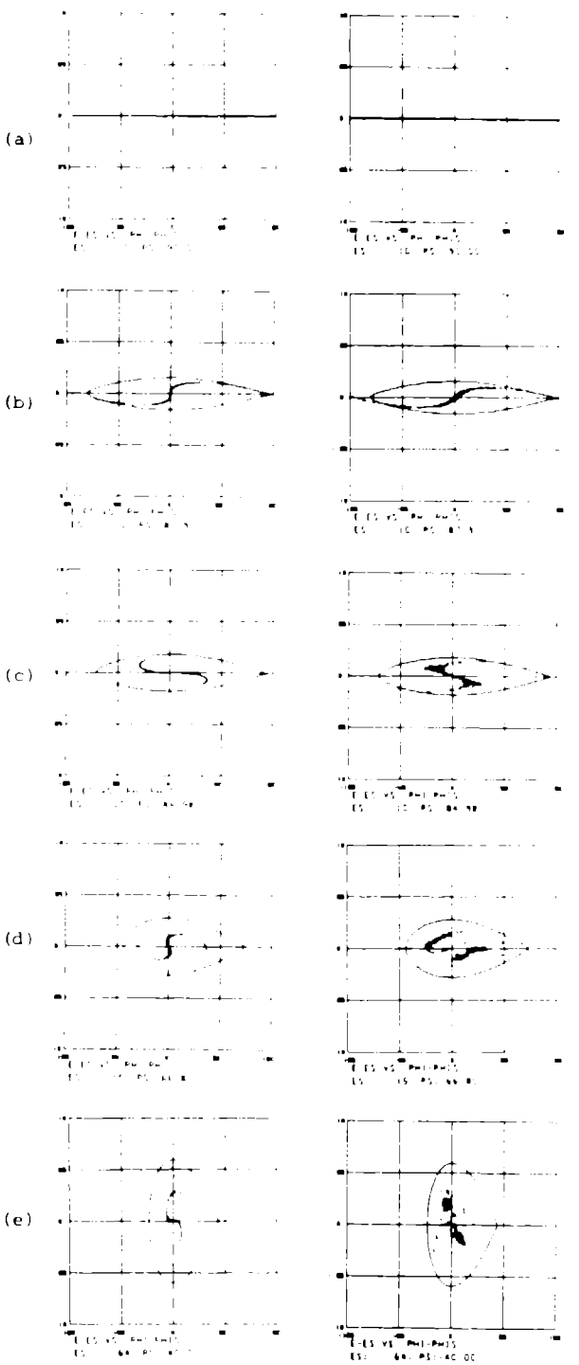

Fig. 8. Longitudinal phase space at center of cell for 425 MHz Test Design.

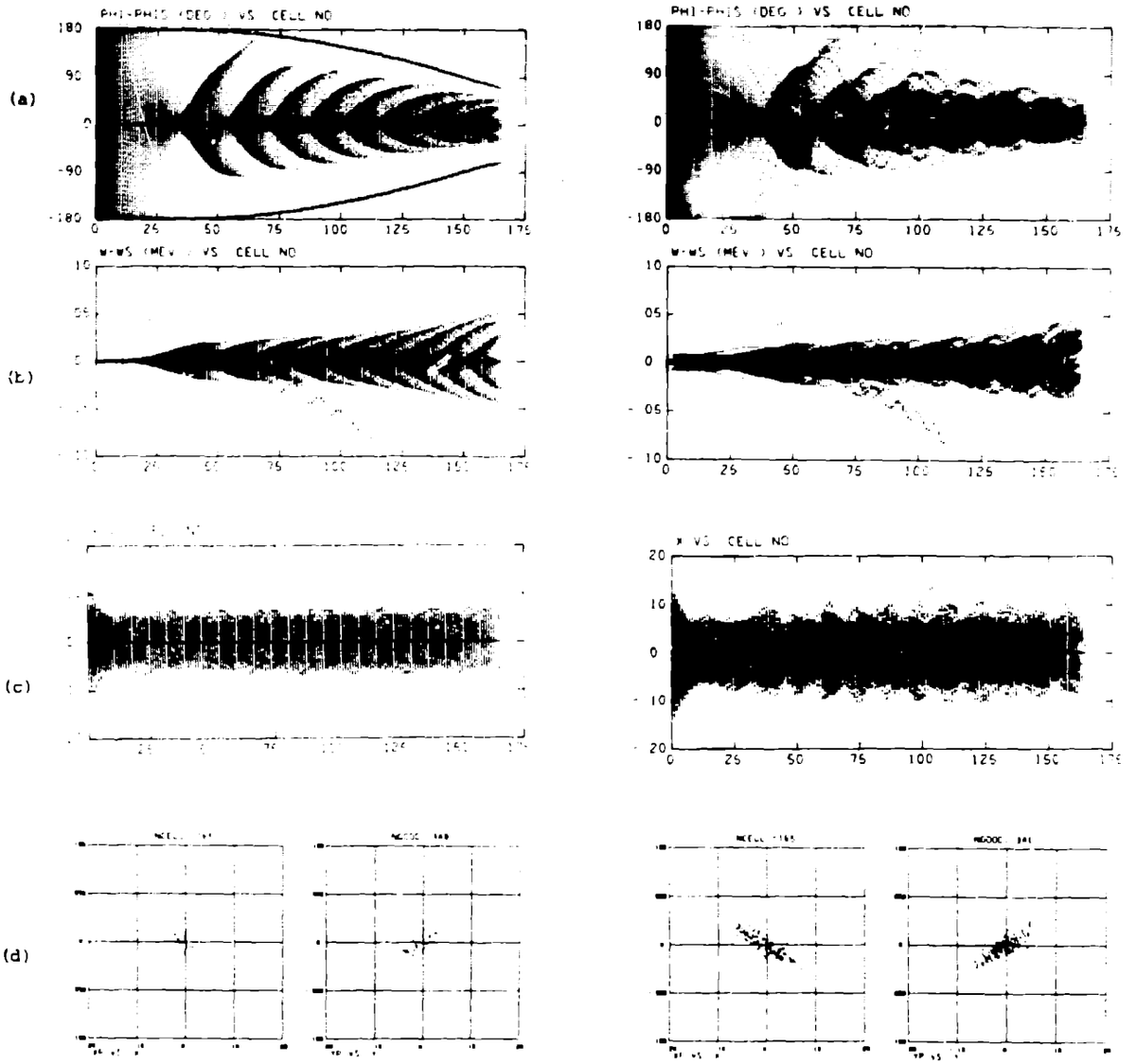

Fig. 7. Results from 425 MHz Test Design.

If we compare the results in Table III with those presented in Table II, we see that the simple linear-ramp approach gives good transmission efficiency when space charge can be neglected. But, as expected, the 425-MHz Test Design is clearly superior in terms of transmission efficency at the nonzero beam currents shown. The radial emittance-growth numbers are significantly perturbed by particle loss at the larger beam currents in both designs.

Acknowledgments

We thank E. A. Knapp, R. A. Jameson, and D. A. Swenson for advice and encouragement. We acknowledge valuable discussions with R. L. Gluckstern, LASL consultant, concerning the Shaper design, and we thank G. W. Rodenz for assistance with the computer calculations.

Appendix

Image Charge Effects

We have tried to estimate the magnitude of the effects on the beam caused by the image charges induced on the vanes by the beam itself. The simplifying assumptions made in this analysis overestimate the image-charge effects.

In the high-energy end of the linac, where the beam is bunched and the vanes have a relatively large modulation, it appears that the image charges actually produce an alternating focusing and defocusing effect for both the longitudinal and radial motions. Although the focusing and defocusing strengths do not necessarily have the same magnitude, the net effect should be less than in the low-energy end, where the main effect is radially defocusing.

The image charges produced by a continuous beam with a circular cross section, centered on axis, will cause multipole fields of order 4, 8, . . ., proportional to the beam current. For a beam with radius r_b, the ratio of the magnitudes of the image force to the space-charge force at the edge of the beam was calculated to be:

$$\frac{\text{image force}}{\text{space-charge force}} = 0.422\left(\frac{r_b}{r_o}\right)^4 + 0.118\left(\frac{r_b}{r_o}\right)^8 + \ldots, \tag{A-1}$$

where r_o is the bore radius. If $r_b = 0.5\ r_o$, then this ratio is less than 3%.

A displacement of the beam center from the axis produces image charges that cause other multipole components, the main ones being the $n = 1$, 3, and 5 terms. The magnitudes of the $n = 4, 8, \ldots$ multipoles are relatively unchanged by small displacements of the beam. The strength of the dipole field is approximately $0.78\ E\ r_c/r_o$, where r_c is the displacement of the beam center from the axis, and E is the space-charge field produced by the beam at a distance r_o from its center. The magnitudes of the $n = 3$ and $n = 5$ multipole fields are each approximately half of the magnitude of the dipole field.

Based on these results, we make the following conclusion: As long as the beam is well centered (say $r_c < 0.2\ r_o$) and the beam does not fill a large fraction of the aperture (say $r_b < 0.6\ r_o$), then the image forces are at least an order of magnitude lower than the space-charge forces and can be neglected without seriously affecting the results. If these conditions are violated, then the image forces might become comparable to the space-charge forces and could cause an increase in the beam loss and in the emittance growth.

Outline of PARMTEQ

The computer program that we use to study the beam dynamics of the RFQ linac is called PARMTEQ, (Phase and Radial Motion in Transverse Electric Quadrupoles). It is a modified version of PARMILA, and performs four basic functions. It generates an RFQ linac, generates a variety of input particle distributions, performs beam dynamics calculations, and generates a variety of outputs.

The information required for generating an RFQ linac consists of the following: the vane voltage; the linac frequency, the mass of the particles; the initial and final energies; and a table of values specifying the radial focusing strength B, the vane modulation parameter m, and the synchronous phase, all at specified distances along the structure. The linac is generated cell by cell, in an iterative procedure.

The beam-dynamics calculations are performed as follows: Each cell is divided into a number of segments (typically four, with a maximum of eight). Initial values of the dynamical quantities x, x', y, y', ϕ, and W are transformed to final values through each segment. The phase and energy coordinates are the first to be transformed. In the radial transformations, the quadrupole and the rf-defocusing terms are treated separately. The quadrupole transformation is that of a standard quadrupole having a length equal to the segment length, and a strength that depends on the rf phase as the particle passes through the segment. Consequently, each particle will experience a different quadrupole force depending on its own phase. The rf defocusing term is treated as an impulse or thin lens, whose strength depends on the rf phase as well as on the location of the particle in the cell.

At the middle of each cell, the particles are given an impulse to simulate the space-charge forces. This is the most difficult transformation to make satisfactorily. In order to calculate properly the space-charge forces, one needs to know the positions of all the particles at a given instant in time. Instead,

one knows the particle coordinates as they arrive at a particular location along the linac. There is a big difference between these two situations when there is a large phase spread in the beam, as there is in the low energy portion of the RFQ. Consequently, before calculating the space-charge forces it is important to estimate the particle positions at a given instant in time, which we have chosen to be the time when the rf field is zero. At this particular time, the cross section of the beam should be very nearly circular. A series of transformation matrices is generated, considering only the quadrupole term, that transforms the radial coordinates from their values at all other phases within $\pm 180^{\circ}$ in 5° increments. For each particle we find the transformation matrix that most nearly agrees with the phase of the particle, and we apply the inverse of the transformation. This gives us the estimate of the particle's radial coordinate at the desired phase. The longitudinal position is estimated from the particle's velocity and phase. After doing this for all of the particles, the space-charge forces are calculated and the impulses are applied by changing x', y', and W for each particle. The radial coordinates are then similarly transformed back to their modified values at their original phases, and this completes the space-charge transformation for one cell.

After the space-charge transformation, the coordinates are transformed through the remainder of the segments in the cell. A variety of output subroutines can be called at the end of any cell, or at the middle of any cell, either before or after the space-charge impulse is applied.

Some RFQ Scaling Methods

Some RFQ applications may require a method of scaling an existing design to some new frequency. At fixed β a change in frequency will cause a change in the operating point on the radial stability chart, which changes the transverse beam dynamics. An exactly equivalent structure may not be obtainable when the frequency is changed. We find that a useful guide for generating solutions at new frequencies is to impose a direct geometric scaling of dimensions in proportion to wavelength. Thus at each cell we have the radius parameter a proportional to λ, and m is unchanged. The frequency dependence of a and E_s tends to make B, Δ, and V decrease as frequency increases and makes E_o increase somewhat with increasing frequency.

For high-current applications of the RFQ it useful to have some means of evaluating the ected importance of space charge effects. We ... t useful to compute the ratio μ of the space ... rge force to the average or smoothed restoring force. We assume a model where the beam bunch is represented by a uniform distribution of charge within a three dimensional ellipsoid. For longitudinal motion we obtain:

$$\mu_\ell = \frac{90\ I(\text{amps})\lambda^3\beta^2 f(b/r_b)}{\pi^2 V(\text{volts}) b r_b^{\,2} A|\sin\phi_s|} \qquad (A\text{-}2)$$

where $r_b^{\,2} = r_x\, r_y$ and b is the half length of the bunch. The function $f(b/r_b)$ has the approximate value $f(b/r_b) = r_b/3b$ in the range $0.8 < b/r_b < 5$.

For radial motion we use

$$\mu_r = \frac{45qI(\text{amps})\lambda\left[1 - f(b/r_b)\right]}{Mc^2(\text{eV})\beta^2 r_b^{\,2} b k_r^{\,2}} \qquad (A\text{-}3)$$

$$\text{where } k_r^{\,2} = \frac{1}{\beta^2\beta^2\lambda^2}\left[B^2 + \beta^2\Delta\right] .$$

Generally we try to keep μ_ℓ and μ_r less than about 0.5 in order to control beam losses due to a reduced stable phase space area. Since μ_ℓ and μ_r affect the frequencies of longitudinal and radial motion, the additional condition must be met, that resonance must be avoided.

We can also obtain limiting current expressions, if we assume the limits occur when $\mu_\ell = 1$ and $\mu_r = 1$. We assume that the bunch half-length is related to the synchronous phase by:

$$b = \frac{\beta\lambda|\phi_s|}{2\pi} \qquad (A\text{-}4)$$

The approximate form for $f(b/r_b)$ is assumed and we replace $\sin\phi_s$ by ϕ_s. For the longitudinal limit we obtain:

$$I_\ell = \frac{AV|\phi_s|^3 r_b}{120\lambda} \qquad (A\text{-}5)$$

where r_b is the beam radius. The radial limit is:

$$I_r = \frac{\beta|\phi_s| r_b^{\,2} Mc^2\left[B^2 + \beta^2\Delta\right]}{720\pi^3\lambda^2 q[1 - f]} . \qquad (A\text{-}6)$$

The longitudinal limit decreases rapidly as the beam is bunched in phase. The radial limit increases with β, but also decreases while the beam is bunched in phase.

At the front end of the RFQ, where the beam is in transition between a DC and a bunched

beam, these formulas will not apply. The lack of separation of bunches will be expected to reduce the longitudinal space charge repulsion, but the conditions arising at each phase focus can create localized unstable regions, where space charge forces may exceed the focusing forces.

References

1. V. V. Vladimirskii, Prib. Tekh. Eksp. No. 3, 35 (1956).
2. G. M. Anisimov and V. A. Teplyakov, Prib. Tekh. Eksp. No. 1, 21 (1963).
3. V. A. Teplyakov, Prib. Tekh. Eksp. No. 6, 24 (1964).
4. P. Fer. P. Lapostolle, C. Beith, and A. Calrespine, Proc. Int. Conf. on Linear Accelerators, Dubna (Aug. 1963), ed. A. A. Kolomensky, A. B. Fusnetsov, and A. N. Lebedev.
5. I. M. Kapchinskii and V. A. Teplyakov, Prib. Tekh. Eksp. No. 2, 19 (1970).
6. I. M. Kapchinskii and V. A. Teplyakov, Prib. Tekh. Eksp. No. 4, 17 (1970).
7. R. H. Stokes, K. R. Crandall, J. E. Stovall, and D. A. Swenson, IEEE Trans. on Nucl. Sci. NS-26, 3469 (1979).
8. J. M. Potter, S. W. Williams, P. J. Humphries, and G. W. Rodenz, IEEE Trans. on Nucl. Sci. NS-26, 3745 (1979).
9. K. R. Crandall, "TRACE: An Interactive Beam-Transport Program," LA-5332, (October 1973).
10. F. Halbach, R. F. Holsinger, W. E. Jule, and D. A. Swenson, "Properties of the Cylindrical RF Cavity Evaluation Code SUPERFISH," Proc. of 1976 Proton Linac Conf., Atomic Energy of Canada Ltd. Report No. AECL-5677, 122 (1976).
11. K. R. Crandall, "Computation of Charge Distribution on or Near Equipotential Surfaces," LA-3512, (December 1966).